



# The vehicle zoom ultra wide angle lens design by using liquid lens technology

Chih-Ta Yen<sup>1</sup> · Jia-Ming Zhang<sup>1</sup>

Received: 6 May 2019 / Accepted: 1 August 2019 / Published online: 12 August 2019  
© Springer-Verlag GmbH Germany, part of Springer Nature 2019

## Abstract

As camera technology develops, products have improved and people have an increasing demand for visual quality. To increase the field of view, many zooming modules have been designed, which has raised the cost of optic components, increased the amount of calculation required, and complicated image processing technology. To date, dashcam lenses are primarily a compensatory design that cannot autozoom. Developing technology with various focuses for use on different roads has become a critical topic for autopilot development. Possibilities include using a short focus on general roads and using a long focus for freeways. Dashcam lens design requires the ability to cover wide angles. The concept behind wide-angle zooming lenses is that when the focal length is the shortest, the widest monitoring range is achieved. To observe a point at a far distance, we can use optical zoom to increase the focal length, thereby enabling a view into the distance. At this time, the angular field of view is sacrificed. However, a reduction of the angular field of view leads to a reduction of distortion, which subsequently reduces the complexity of back-end image processing and leads to clearer images. The design in this study references the wide-angle lens patent US.20090080093 (Ning in Compact fisheye objective lens, U.S., Patent No. 20090080093, 2011) of Alex Ning, whose optical system consists of six spherical lenses. The angular field of view reached 170°. The total system length is 18 mm, and F/# is 3. The system focus is 1.652 mm. Four groups of liquid lenses were placed in this wide-angle lens. Altering the curvature and thickness of the liquid lenses changes the course of light and forms a new angular field of view. This system consists of three zoom settings, with fields of view being 170°, 160°, and 150°, respectively. The F/# was 2.4. The modulation transfer function at a spatial frequency of 1801 p/mm reached 6%, 0%, and 27%, respectively. F-Theta was controlled within  $\pm 10\%$ . The spot size was smaller than 4  $\mu\text{m}$ , and the field curvature was smaller than  $\pm 0.02$  mm. The liquid lenses were successfully introduced into the wide-angle lens to achieve optical zoom without using a conventional mobile mechanical structure.

## 1 Introduction

A wide-angle lens refers to a lens with an angle of view larger than 55° or with a focal length smaller than 35 mm. It is commonly used in general photography to satisfy photographers' needs. If there is a need for an even wider angle of view, wider than 120°, then the lens is called an ultra-wide-angle lens. These are typically used in dashcams and security monitors. The purpose of using an ultra-wide-angle lens is to observe a wide range of area simultaneously. The lens with an angle of view close to or even exceeding 180° is called a fisheye lens. In sum, according

to angle of view, lenses can be classified as standard, wide-angle, ultra-wide-angle, and fisheye, each of which can be used in different situations to satisfy user needs. Before designing a wide-angle lens, we must have a certain understanding of fisheye lenses. Fisheye lenses were designed because humans wanted to imitate the view of a fish underwater looking up to the surface with the upper hemisphere of its eyes. From fisheye lens, we can understand the design principle of ultra-wide-angle lenses.

Ultra-wide-angle lenses were designed by Wood. He placed a glass plate on a container filled with water to form a pinhole camera to actualize ultra-wide-angle photography. By opening a hole on the surface of water as the grating of the lens, he observed the image from the bottom of the container. This method was inconvenient because it required having a water tank around, so Bond further improved upon Wood's device. Bond used a hemispherical

✉ Chih-Ta Yen  
chihtayen@gmail.com

<sup>1</sup> Department of Electrical Engineering, National Formosa University, Yunlin County 632, Taiwan

glass lens to replace the water tank. At the center of the surface of the hemispherical glass ball, he left a small hole as the grating. Bond's device only used a flat convex lens to capture an image and did not feature any optical component to reduce aberrations, so the image quality was unsatisfactory. Hill (1926) improved upon Bond's structure by adding a negative concave lens to increase the curvature of Bond's lens to effectively increase the amount of light let in. Because of the negative concave lens added to the front, the incident angle was reduced from  $90^\circ$  to  $60^\circ$ , which effectively increased image quality. Therefore, the device Hill developed became the prototype for fisheye lenses. Subsequent fisheye lenses or ultra-wide-angle lenses were all developed on the basis of this structure. In 1924, Beck (1925) improved upon Hill's lens by adding a lens to increase the degree of freedom to adjust aberration. He used a concave lens to adjust the aberration of fisheye lenses. A concave lens can reduce the incident angle of light from large angles into the set of lenses, thereby effectively increasing the amount of light let in. Because the number of lenses increased, the size of the aperture was increased to F/22. The fisheye lens designed by Schulz (1932) aimed to reduce the angle between the chief ray and the optic axis; thus, two negative concave lenses were placed in the front and a set of doublet lenses were placed in front of the aperture grating. Behind the grating were a flat glass and a biconvex lens instead of a hemisphere plane-convex lens to increase the degree of freedom. As a result, the image quality was better than earlier models. Fisheye lenses and ultra-wide-angle lenses have been applied in various situations. Zheng and Li (2006) used fisheye lenses for scenery scanning. Wei et al. (Feng et al. 2011) incorporated them into cars as assistive lenses. Huang et al. (2010) designed a multiple-spectrum fisheye lens for rice paddy assessment. The use of wide angle and fish-eye lenses always causes strong distortions in the resulting images. The approach (Brauer-Burchardt and Voss 2001) proposed is based on circle fitting algorithm of the extraction of distorted image points from straight lines in the 3D scene.

Because of the need to meet specifications, optic designers often design lens structures with a single fixed effective focus lens (EFL) to obtain optimal image quality during a simulation period. However, when an object is required to be enlarged or reduced, depending on the distance of the photography subject, users have to approach or back away from the object with the lens to suit their need when using a fixed EFL. Therefore, a zooming camera is convenient for photographing objects at various distances. The design of zooming lenses with multiple EFLs enables the lens system to take in objects at various distances (Mikš et al. 2008; Wick et al. 2005). A zooming system is a highly complex optical system (Martinez et al. 2004;

Johnson and Feng 1992). Conventional zooming lenses (Kienholz 2011) are composed of a front lens set, a zooming lens set, a back lens set, and a compensatory lens set. The focusing and zooming of light is achieved through movement of the lens sets. However, when a lens set is too complicated, the weight of the camera becomes too heavy. Long-term use results in damage to the mechanical structure and subsequently reduces precision. If liquid lenses are used in lens zooming and their curvature and thickness can be altered by altering voltage, pressure, and temperature to achieve zooming, this can reduce the length and weight of the lens set. Liquid lenses can zoom and be used in microelectromechanical systems. They use an imaging system and optical communication system for autofocusing and zooming. Compared with a conventional camera with a mobile and complex mechanical set of lenses, liquid lenses can focus and zoom faster using less power.

## 2 Liquid lenses design and specification

The history of liquid lenses can be traced back to 1995 when MAN SE used the first liquid lens for an electrowetting display. In 2004, Philips exhibited liquid lenses at the CeBIT expo. Subsequently, numerous companies became involved in the research and development and production of liquid lenses. The French companies Varioptic, HoloChip, and Optotune produced several commercial liquid lenses in the United States. They have different specifications for different applications. The products from the three companies include those demonstrated in (Blum et al. 2011). Several methods have been used to make liquid lens components, namely applying pressure (Ren and Wu 2007), using thermal effect (Dong et al. 2006), dielectrophoresis (Ren and Wu 2008), and electrowetting (Berge and Peseux 2000). In Ren and Wu (2007), the liquid lens had two bases to seal the external surface of the aperture at the top and the elastic membrane of the inner surface of the hole at the bottom. When pressure is applied to the external membrane, the liquid within is reallocated, resulting in the expansion of the inner membrane that serves as the plano-convex lens. In Dong et al. (2006), the liquid lens used liquid that was thermal sensitive. A heat effect was applied to change the surface curvature. In Ren and Wu (2008), the dielectrophoretic phenomenon was utilized to create force to push liquid to an adjacent hole. Curvature difference was created using tuning voltage. The lens with electrowetting liquid (Berge and Peseux 2000) uses two different types of liquids, one that is electrically conductive and that is not. When tuning voltage is altered to change the electric field, the liquid that is electrically conductive changes the surface curvature between the two liquids. Electrowetting liquid lenses have various

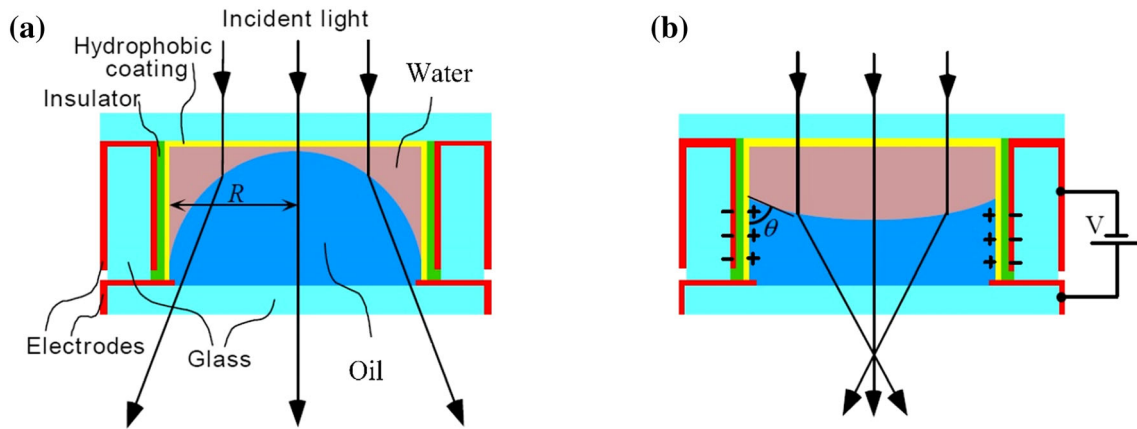


**Fig. 1** Liquid lens states **a** without applying voltage and **b** applying voltage (Kuiper et al. 2004)

applications (Fang and Tsai 2008; Fang et al. 2011; Sun et al. 2009). The research (Yen and Shih 2015) proposes using a liquid lens as a compensating lens and applying intermediate optics to achieve a  $9\times$  zoom ratio. The droplet shape and location of the liquid lens can be adjusted reversibly, enabling the focal length and position of the lens to be tuned by varying the voltage applied to a set of electrodes.

The present study discusses the application of liquid lenses. First, electrowetting liquid lenses are analyzed. The phenomenon of electrowetting was identified in 1875 (Lippmann 1875). Figure 1 is a schematic of an electrowetting liquid lens in which the cylindrical shell contains two liquids that do not mix and have different refractive indices. One liquid is electrically conductive, whereas the other one is insulative. The two liquids are typically water and oil. By changing the voltage applied to the cylindrical shell, the contact angle of the two liquids changes, thereby affecting the curvature of the contact surface. Therefore, the optical power of the lens is altered with various voltage levels. Electrowetting liquid lenses exhibit characteristics such as a large range of power, fast response, and a long life, whereas the main shortcomings are high drive voltage and limited aperture size.

Liquid lenses can be used for automatic focusing in the optical system. Compared with a conventional automatic focusing system, liquid lenses achieve a faster and more accurate autofocusing system. Liquid lenses also have a higher circulation life and consume less power. One application of liquid lenses is in wide-angle lens for optical zooming, which is the main focus of this study. We used two or more liquid lenses to create a zooming system. Many studies have focused on this topic. Figure 2 demonstrates the zooming system with two sets of liquid

lenses designed by Kuiper (2007). Kuiper and Blum discussed the application of liquid lenses in medical devices, such as endoscopes and microscopes (Blum et al. 2011). Hao et al. (2013) used two zooming components to analyze the theory of a first-order optical zooming lens.

Zoomable liquid lenses have been widely used commercially in the past few years. However, the range of applications is still limited. Due to the hard work of various researchers and engineers, the performance of liquid lenses has increased rapidly. It is foreseen that liquid lenses will become even more crucial in lens design, especially in optical systems that require rapid performance. To use liquid lenses as zooming lenses, several points must be addressed. First, the negative power of the zooming optic fixes the curvature of the field, which subsequently reduces the modulation transfer function (MTF). Second, the Abbe number of liquid optical material is different from dispersive optical material, so the color difference in the axial direction is severe. Third, the primary light ray may be bent substantially to adjust to the limited liquid optical aperture, resulting in increased aberration that could complicate optical design (Zhang et al. 2013).

This study used the ARCTC-416 liquid lens, produced by Varioptic and whose structure is presented in Fig. 3. It is mainly composed of two glass pieces encircling two liquids (Liquids A and B). Voltage differences were used to alter the curvature between the two liquids. The actual structure of the ARCTC-416 is shown in Fig. 4. The thickness of Glasses 1 and 2 were 0.55 mm and 0.3 mm, respectively. The thicknesses of Liquids A and B were both 0.65 mm.

The specification is that Glass 1 = Glass 2. The index of refraction under each wavelength is shown in Table 1. The index of refraction of Liquids A and B is shown in Table 2.

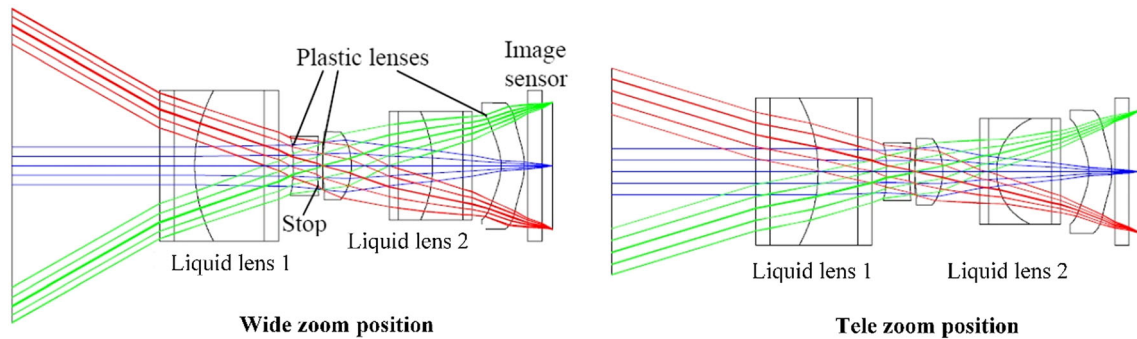


Fig. 2 Zooming system with two sets of liquid lenses designed by Kuiper et al. (2007)

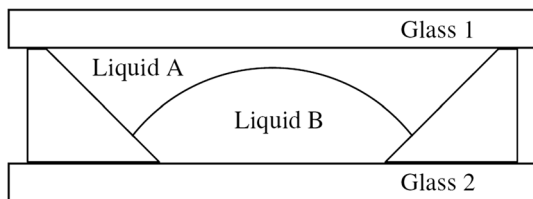


Fig. 3 Side view schematic of the liquid lens structure (Varioptic 2006)

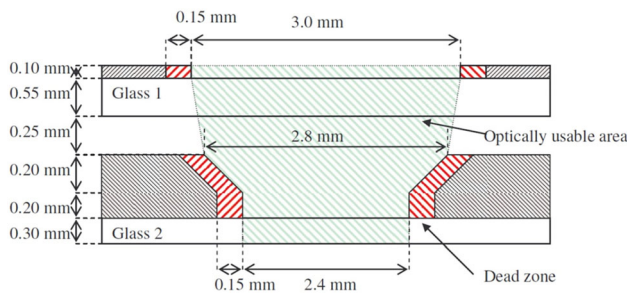


Fig. 4 Schematic of liquid lens structure (Varioptic 2006)

The influence of voltage on the curvature and thickness of Liquids A and B is shown in Table 3.

### 3 Sensor and lens specifications

In this study, the complementary metal–oxide–semiconductor (CMOS) image sensor used was the OmniVision OV2722, whose effective picture pixels are  $1932 \times 1092$  and total resolution is 210 million pixels. A single pixel size is  $1.4 \mu\text{m} \times 1.4 \mu\text{m}$ . The specification of the sensor is shown in Table 4 (OmniVISION 2012).

Among the items used to evaluate the quality of a lens, the most critical ones are resolution and sharpness. At a low spatial frequency, a high MTF means the camera has favorable contrast and can show a clear outline. At a high spatial frequency, high MTF means the camera image is sharp and exhibits more detail. The spatial frequency of a CMOS image sensor is related to pixel size. Nyquist

Table 1 Relationship between wavelength and index of refraction of the glass (Varioptic 2006)

$\lambda$ (nm)	Index
700.0	1.5150
650.0	1.5164
590.0	1.5187
550.0	1.5206
480.0	1.5252
430.0	1.5300

Table 2 Index of refraction of the liquid lens (Varioptic 2006)

Wavelength (nm)	Liquid A	Liquid B
400	1.41178	1.5127
448	1.40729	1.5034
489	1.40451	1.49772
541	1.4018	1.4925
589.3	1.39988	1.48894
654.6	1.39791	1.48535
703	1.39671	1.48332

frequency can be obtained from Eq. 1 (Edmund Optics Inc 2014).

$$MTF = \frac{1}{4 \times \text{pixel size (mm)}} \quad (1)$$

Because the size of a single pixel was  $1.4 \mu\text{m}$ , the maximum spatial frequency was 1781 p/mm. To obtain favorable imaging quality, we hoped that the spatial frequency could reach 1781 p/mm more than 10% of the time.

After CMOS was set, height (h) = 1.56 mm because the height (h) is half of the length of the diagonal line. However, in general optical design, to prevent dark corners, the design must extend outward for 80 pixels. After calculation, the new height could be obtained. The new length of the diagonal line is the original length plus the length of 80 pixels. We divided the new length by 2 and obtained the new design image height of approximately 1.6 mm.

**Table 3** Curvature and thickness for two liquid lenses

Voltage (V)	R (mm)	PC100 (Liquid A) thickness (mm)	H100 (Liquid B) thickness (mm)
0–29	– 8.54	0.392	0.258
30	– 8.705	0.390	0.260
31	– 9.429	0.385	0.265
32	– 10.308	0.380	0.270
33	– 11.394	0.374	0.276
34	– 12.770	0.369	0.281
35	– 14.565	0.363	0.287
36	– 17.006	0.357	0.293
37	– 20.509	0.352	0.298
38	– 25.959	0.346	0.304
39	– 35.587	0.340	0.310
40	– 57.163	0.334	0.316
41	– 149.088	0.328	0.322
42	234.978	0.322	0.328
43	64.966	0.316	0.334
44	37.453	0.310	0.340
45	26.195	0.304	0.346
46	20.074	0.298	0.352
47	16.23	0.292	0.358
48	13.592	0.286	0.364
49	11.67	0.279	0.371
50	10.209	0.273	0.377
51	9.060	0.267	0.383
52	8.134	0.260	0.390
53	7.372	0.254	0.396
54	6.734	0.247	0.403
55	6.193	0.241	0.409
56	5.727	0.234	0.416
57	5.323	0.227	0.423
58	4.969	0.221	0.429
59	4.656	0.214	0.436
60	4.378	0.207	0.443

**Table 4** Complementary metal-oxide-semiconductor specification

Active array	1932 × 1092
Pixel size	1.4 μm × 1.4 μm
Image area	2.7 mm × 1.5 mm
Device diagonal	3.133 mm
Chief ray angle	28°

**Table 5** Calculation results under each zooming setting

Zoom	FOV (deg)	efl (mm)	h (mm)
1	170	1.184	1.6
2	160	1.244	1.6
3	150	1.314	1.6

We designed three degrees of zooming. The fields of view (FOVs) were 170°, 160°, and 150°. However, in an optical system with a large angle, barrel distortion is substantially generated to produce an image on the limited imaging plane. Consequently, the equation  $h = f \tan \theta$  cannot be used because this equation is a near-axis

equation and will be negated by large distortion. As a result, the projection imaging method was adopted for the design of the present study (Lin 2008; James et al. 2000). We substitute the FOV angle into the solid angle projection imaging equation  $h = 2f \sin(\frac{\omega}{2})$ , where  $h = 1.6$  mm and  $\omega$  is the half-FOV angle 85°, 80°, and 75°. After calculation,

**Table 6** Data about four groups of liquid lens sets

Surface# Object	Curvature radius (mm) Infinity	Thickness (mm) Infinity	Material
1	9.515887	1.596325	H-ZLAF68A
2	3.257733	2.736808	
3	– 14.042711	0.697770	N-LAK33
4	3.449215	0.899670	
5	12.672020	3.366030	H-ZF52A
6	– 10.236089	1.329981	
Liquid Lens 1			
7	Infinity	0.550000	GLASS1
8	Infinity	0.334000	PC100
9	– 57.163000	0.316000	H100
10	Infinity	0.300000	GLASS2
11	Infinity	1.032922	
LiquidLens 2			
12	Infinity	0.550000	GLASS1
13	Infinity	0.286000	PC100
14	13.592000	0.364000	H100
15	Infinity	0.300000	GLASS2
16	Infinity	0.047771	
STOP	Infinity	0.048556	
18	6.804041	0.966619	LAF3
19	– 6.869258	0.048088	
20	6.364938	0.799602	H-LAK51
21	– 2.989867	1.255628	H-ZF62
22	– 23.690657	0.048170	
Liquid Lens 3			
23	Infinity	0.550000	GLASS1
24	Infinity	0.279000	PC100
25	11.670000	0.371000	H100
26	Infinity	0.300000	GALSS2
27	Infinity	0.254948	
LiquidLens 4			
28	Infinity	0.550000	GLASS1
29	Infinity	0.260000	PC100
30	8.134000	0.390000	H100
31	Infinity	0.300000	GLASS2
32	Infinity	0.045074	
33	Infinity	0.300000	H-K9L
34	Infinity	0.490275	
Image	Infinity		

the effective focus length ( $efl$ ) of each zooming section was obtained (Table 5).

#### 4 Lens arrangement and image quality

Table 6 presents lens data of zooming wide-angle lenses. Table 7 displays the zooming parameters of each zooming section; different zooms correspond to different curvature

radii and thicknesses. Figures 5, 6 and 7 are the three-dimensional (3D) layouts of Zooms 1, 2, and 3 with FOVs = 170°, 160°, and 150°, respectively. The aforementioned 3D layout systems all have a total system length of 21.9124 mm.

The following shows the MTFs of the three zooms. The x-axis represents spatial frequency, and the y-axis denotes the MOF. The resolution of each FOV at a different spatial



**Table 7** Zooming parameters of four sets of liquid lenses

Zoom	Curvature radius (mm)				Thickness (mm)							
	S9	S14	S25	S30	S8	S9	S13	S14	S24	S25	S29	S30
1	− 57.163	13.592	11.67	8.134	0.334	0.316	0.286	0.364	0.279	0.371	0.26	0.39
2	6.193	− 25.959	26.195	16.23	0.254	0.396	0.346	0.304	0.304	0.346	0.292	0.358
3	4.378	− 20.509	− 8.54	− 8.705	0.207	0.443	0.352	0.248	0.392	0.258	0.39	0.26

**Fig. 5** 3D layout of Zoom 1

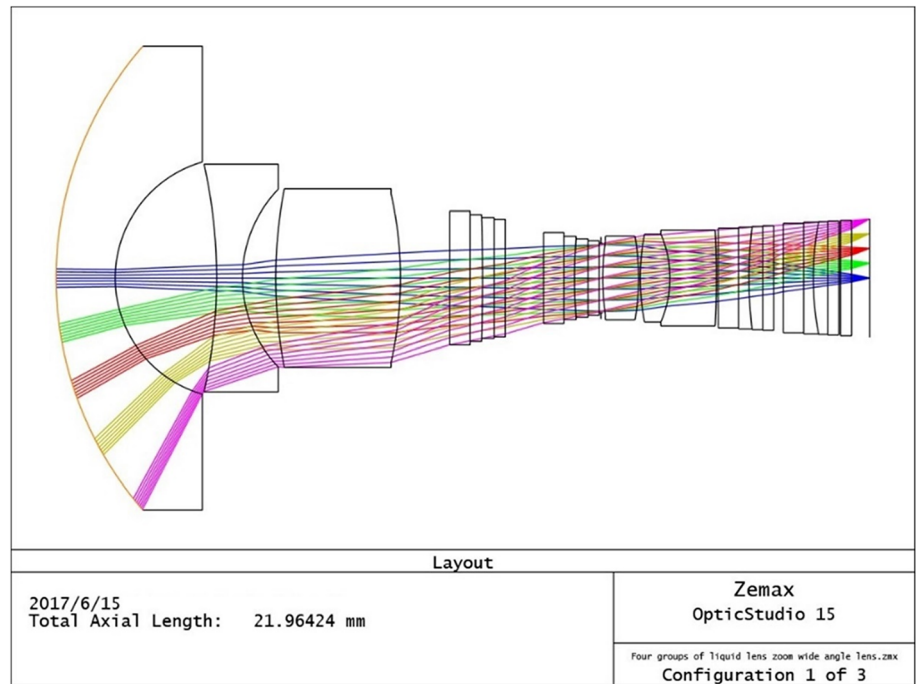


**Fig. 6** 3D layout of Zoom 2

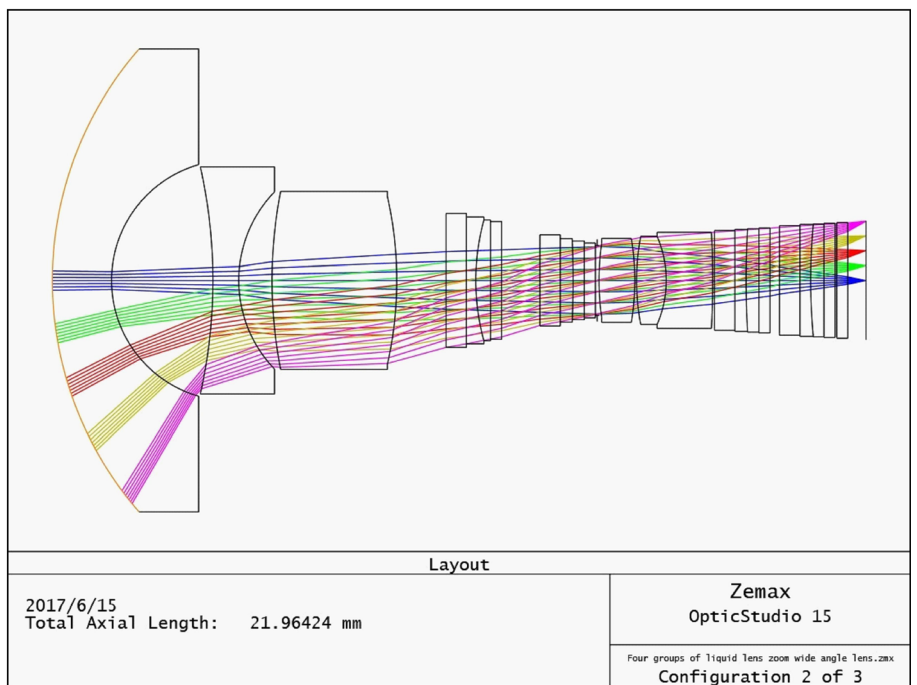
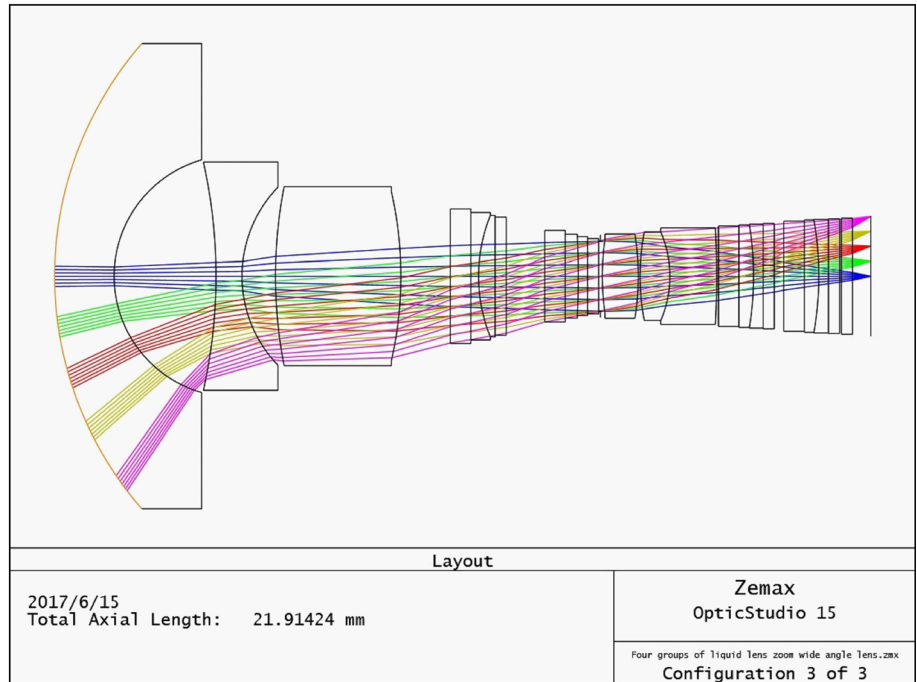


Fig. 7 3D layout of Zoom 3



frequency is shown in the figures. Figures 8, 9 and 10 are the MTFs of Zoom 1, Zoom 2, and Zoom 3, respectively.

Table 8 shows that for Zoom 1, Zoom 2, and Zoom 3 at the spatial frequency of 1801 p/mm, their MTFs reached 6% or higher, 30% or higher, and 27% or higher,

respectively. Clearly, the MTFs of Zoom1 were not ideal, and Zoom 2 and Zoom 3 were much superior with MTFs reaching approximately 30%. The light spot diagram reflects the size of the light vector on the imaging plane, which is the density of the energy from a point source of

Fig. 8 MTF of Zoom 1

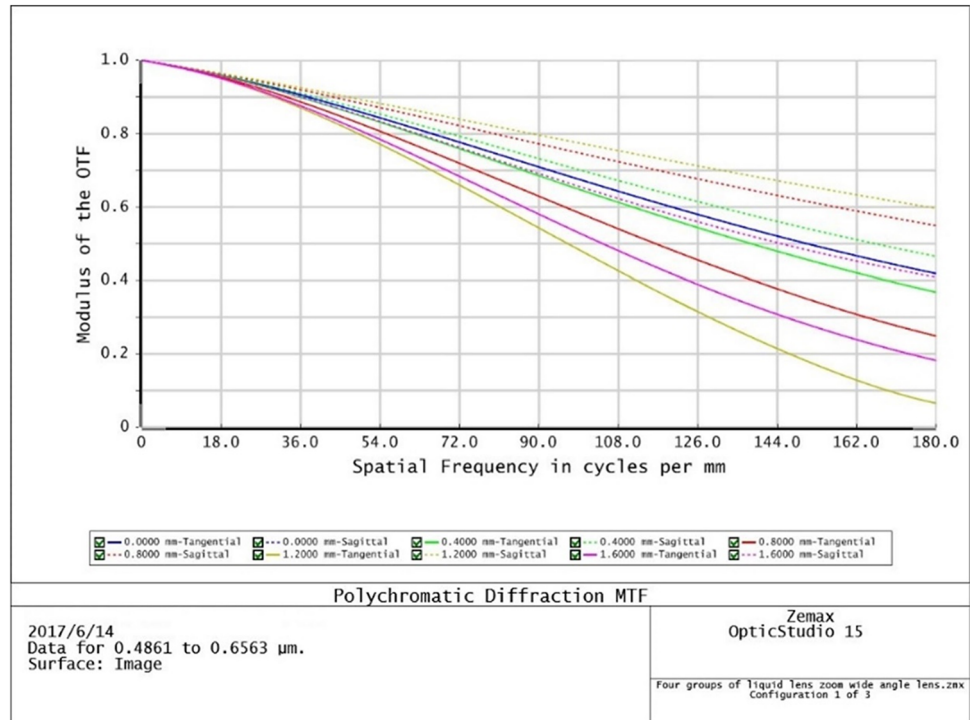
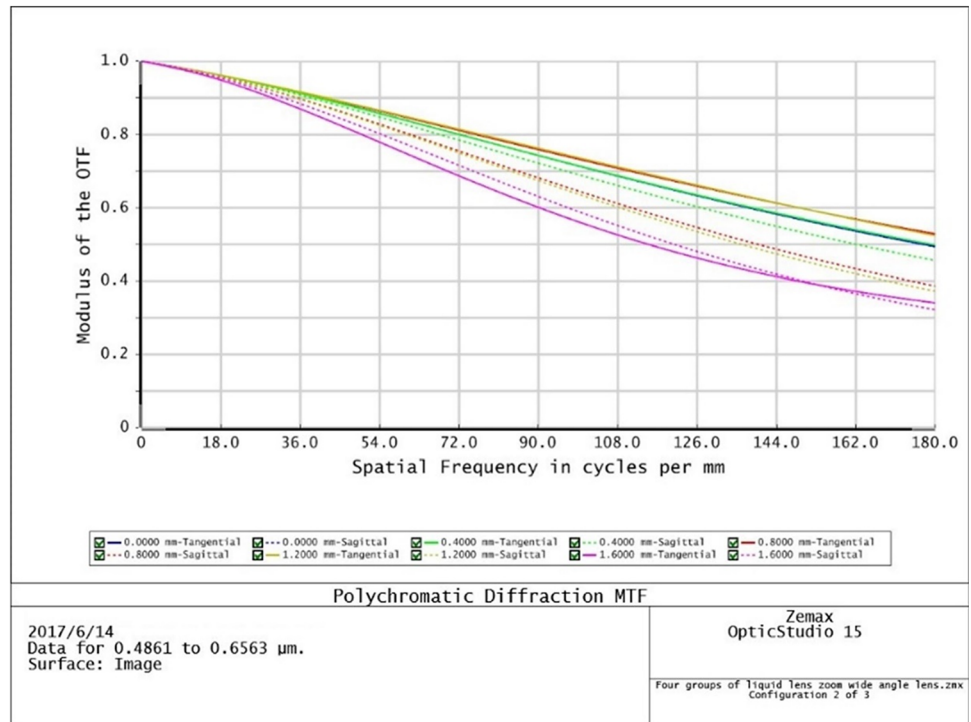




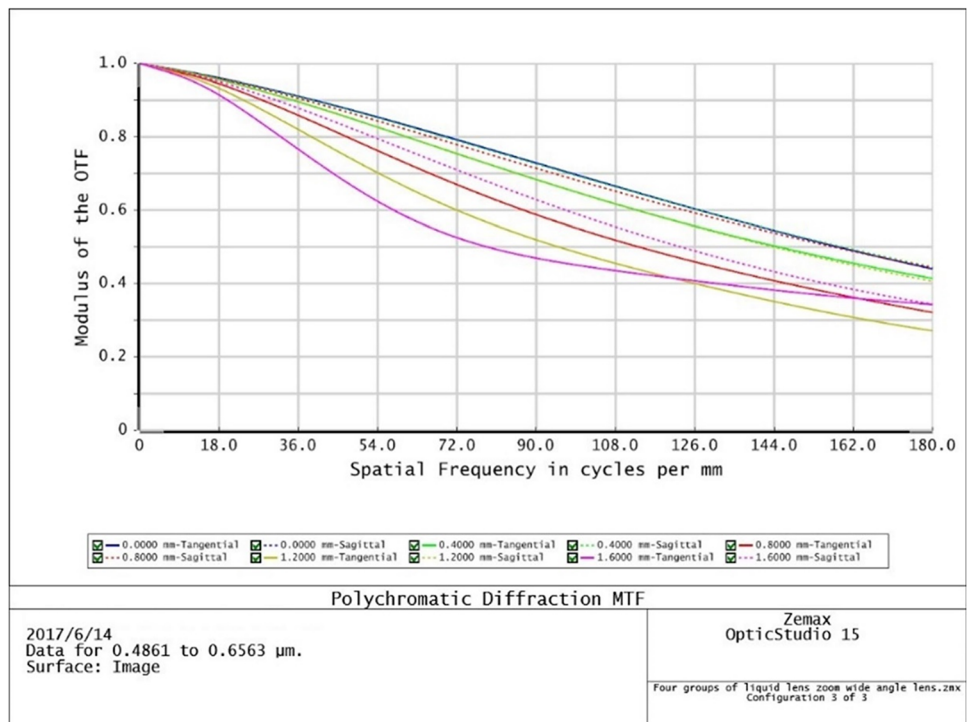
Fig. 9 MTF of Zoom 2



light. Figures 11, 12, and 13 are the spot diagrams of Zoom 1, Zoom 2, and Zoom 3, respectively. The figures show that the energy under the blue wavelength in Zoom 1 and Zoom

3 was not dense, whereas the energy under the red wavelength in Zoom 1 was not dense. In the spot diagrams, the spot RMS radius in each zoom does not exceed 4  $\mu\text{m}$ .

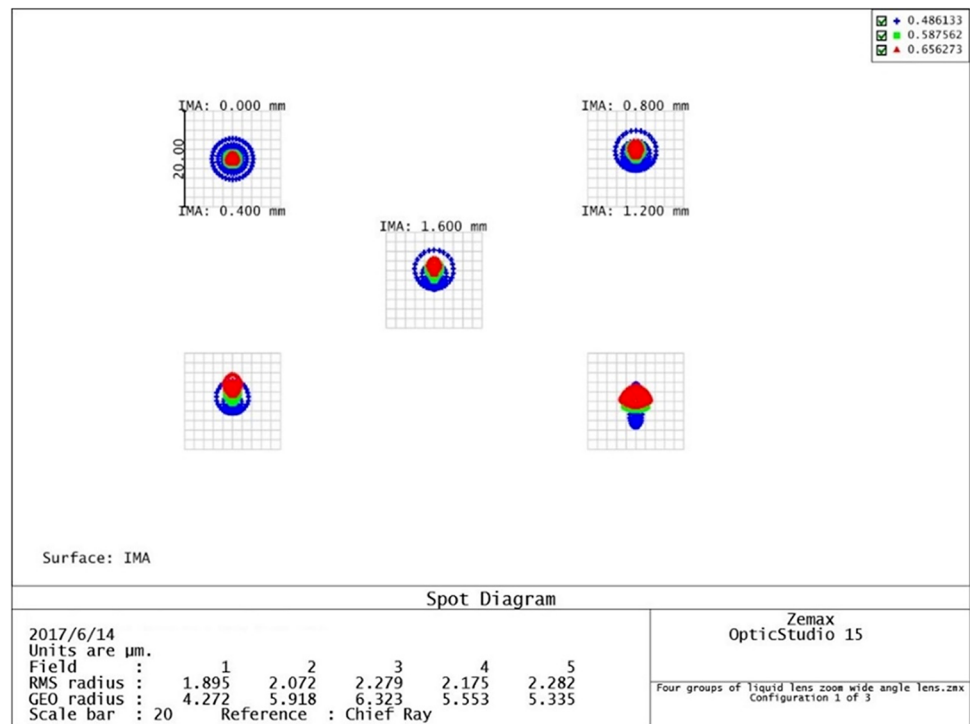
Fig. 10 MTF of Zoom 3



**Table 8** MTF data

Zoom	Spatial frequency of 180 lp/mm MTF		
	Field (mm)	Tangential	Sagittal
1	0	0.418624	0.418624
	0.4	0.368001	0.465380
	0.8	0.248792	0.549357
	1.2	0.065208	0.596364
	1.6	0.181979	0.408643
2	0	0.493922	0.493922
	0.4	0.498300	0.455985
	0.8	0.528827	0.386485
	1.2	0.523969	0.372630
	1.6	0.340899	0.321999
3	0	0.439975	0.439975
	0.4	0.414022	0.445126
	0.8	0.320872	0.442995
	1.2	0.270774	0.406205
	1.6	0.342822	0.343174

The figures on the left display the field curvature at each wavelength. The y-axis shows the imaging height of light, and the x-axis denotes the differences between the focusing

**Fig. 11** Spot diagram of Zoom 1

locations of paraxial and off-axis rays. The figures on the right show F-Theta distortion. The y-axis denotes the imaging height of light, and the x-axis shows the differences in percentage of the actual light and the paraxial light focusing on the imaging plane. This figure also reveals the half-FOV (HFOV) of the system. Figures 14, 15 and 16 show that the HFOVs of Zoom 1, Zoom 2, and Zoom 3 were 84.980, 80.05, and 74.97, respectively.

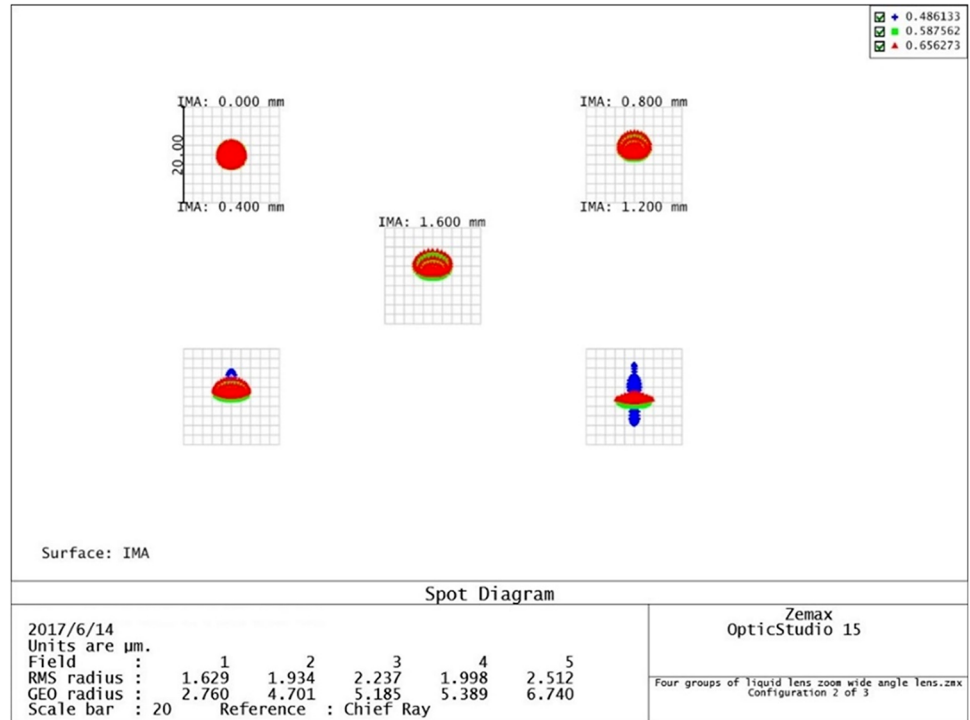
Table 9 reveals that the reduction of FOV mitigated distortion, and the F-Theta of each Zoom under each wavelength was controlled to under 10%.

Table 10 summarizes the aforementioned simulation results, and the optical performance of each zoom can be observed.

## 5 Conclusion

The present study used liquid lenses for optical zooming. Four groups of liquid lenses were used in wide-angle lenses. This optical zooming system relied on the alteration of the curvature and thickness of liquid lenses. This system consisted of three zoom settings, with FOVs of 170°, 160°, and 150°. The F/# was 2.4. The MTF at a spatial frequency of 1801 p/mm reached 6%, 0%, and 27% for Zoom 1, Zoom 2, and Zoom 3, respectively. F-Theta was controlled

**Fig. 12** Spot diagram of Zoom 2



**Fig. 13** Spot diagram of Zoom 3

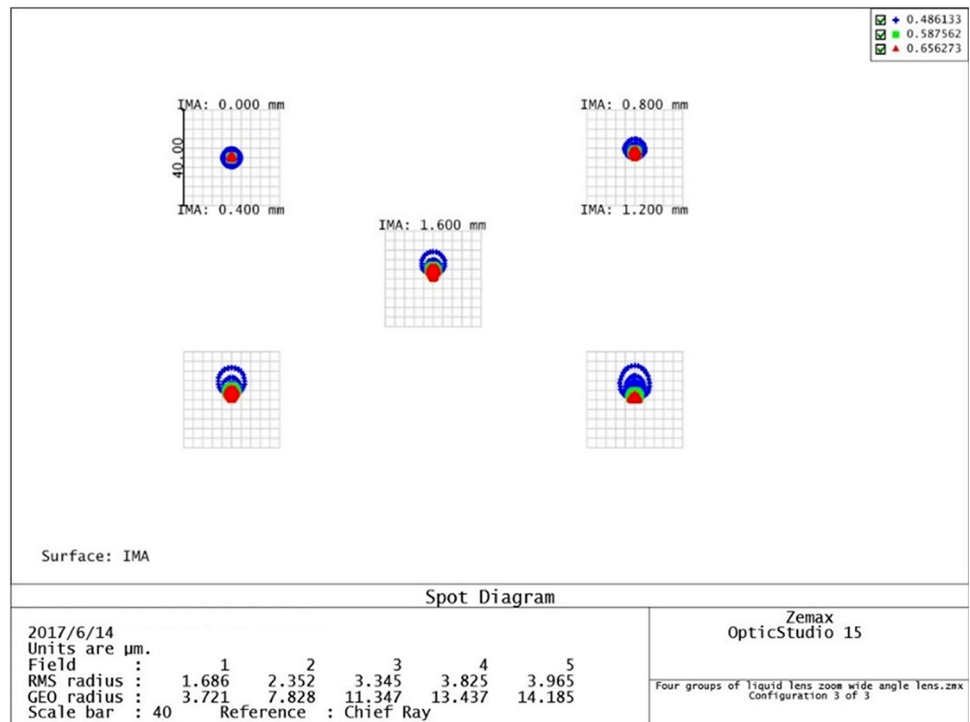


**Fig. 14** The field curvature—F-theta distortion graph of Zoom 1

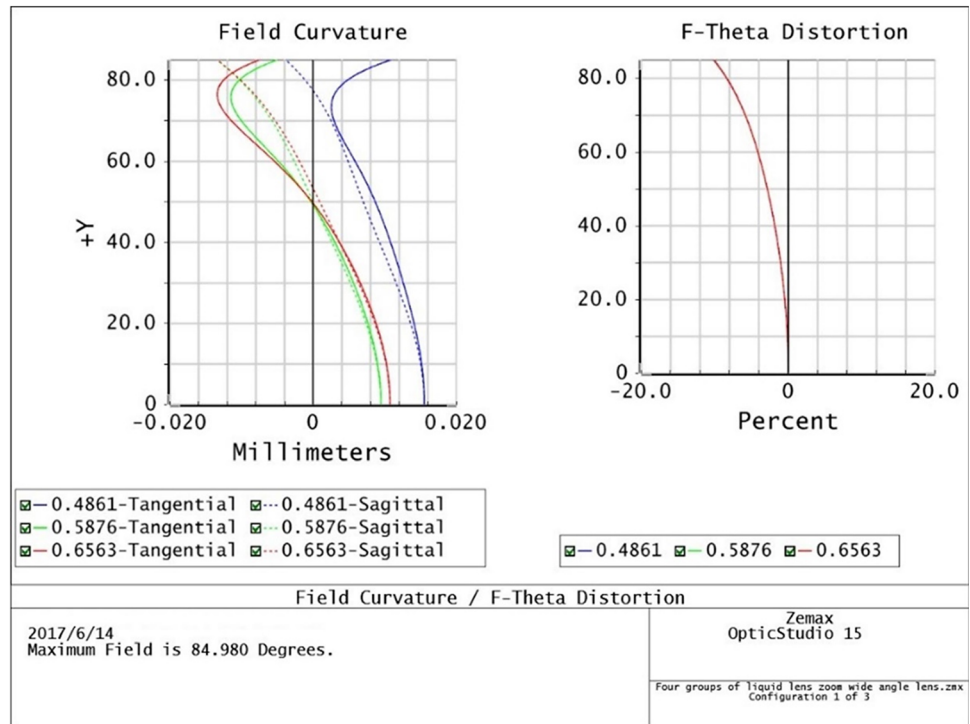


**Fig. 15** The field curvature—F-theta distortion graph of Zoom 2

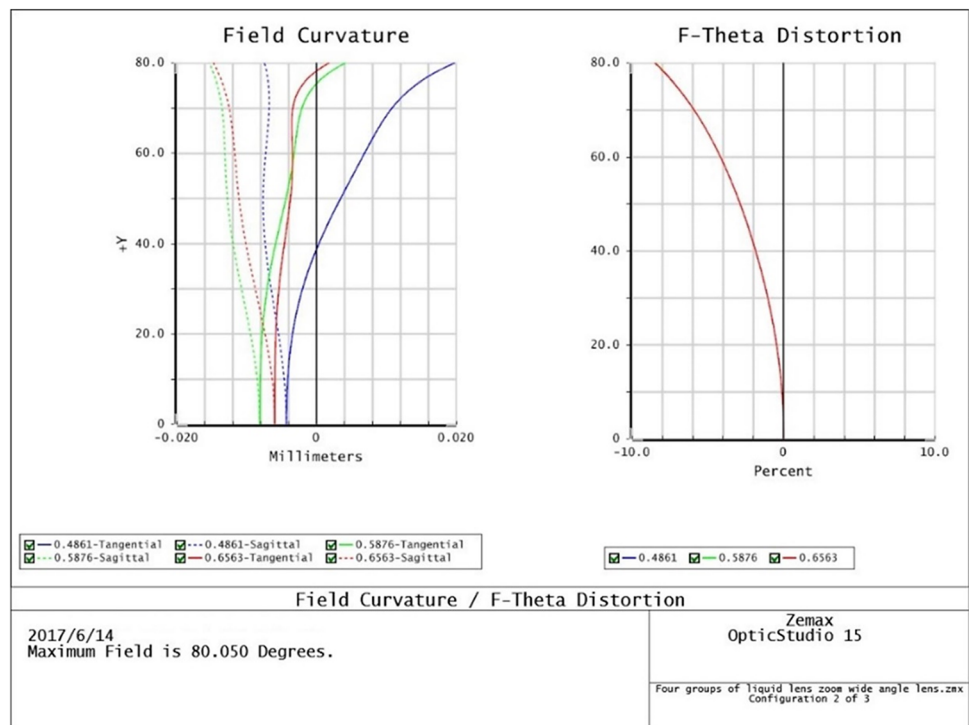


**Fig. 16** The field curvature—F-theta distortion graph of Zoom 3

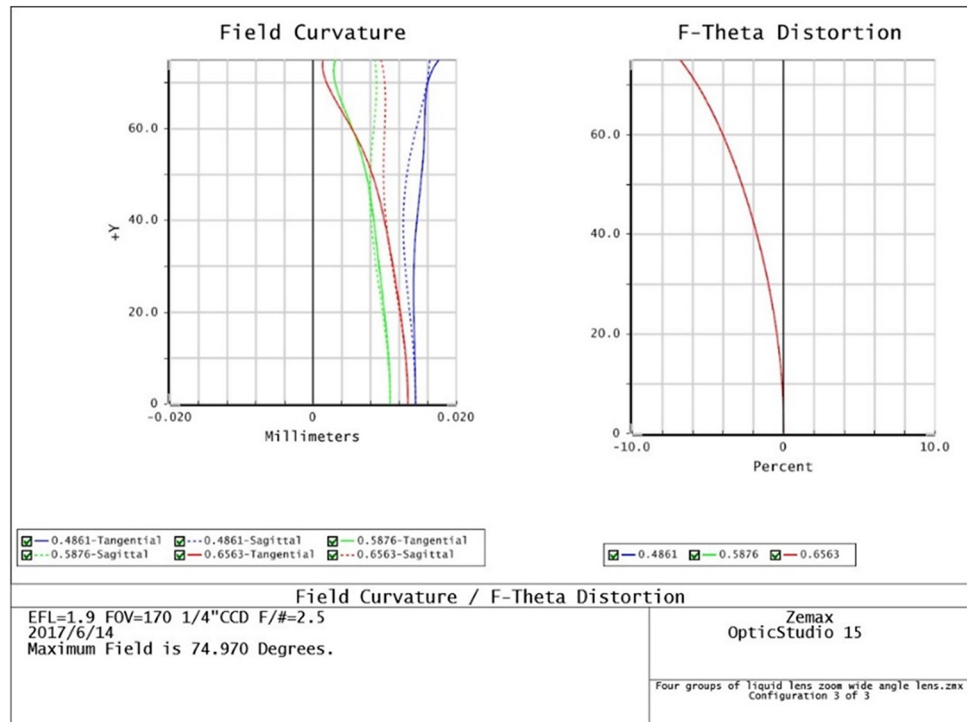


**Table 9** F-Theta distortion data

Zoom	F-Theta distortion		
	Wavelength (μm)		
	0.486133	0.587562	0.656273
1	− 10.04192377%	− 10.11598158%	− 10.15365437%
2	− 8.44957409%	− 8.48133255%	− 8.50032753%
3	− 6.80122398%	− 6.82282636%	− 6.83578993%

lens to achieve optical zoom without using a conventional mobile mechanical structure. We demonstrated the concept of wide-angle zooming lenses. However, limited by the focus range and the size of the aperture, the imaging quality could hardly be balanced in the performance of each group. Perhaps in the future, with increased degrees of freedom in the focus and aperture of liquid lenses, the design limitation can be reduced and the image quality can be improved.

within 10%. The spot size was smaller than 4 μm, and the field curvature was smaller than ± 0.02 mm. The liquid lenses were successfully introduced into the wide-angle

**Table 10** Zooming results of four groups of liquid lenses

Item	Results		
Zoom	1	2	3
HFOV (deg)	85	80	75
F/#	2.4	2.4	2.4
Total Length (mm)	21.9642	21.9642	21.9642
EFL (mm)	1.20	1.25	1.31
MTF	180 lp/mm > 27%	180 lp/mm > 30%	180 lp/mm > 6%
Spot size (μm)	< 4	< 2.5	< 2.3
F-θ (%)	< ± 10	< ± 10	< ± 10

**Acknowledgements** This study was supported in part by the Ministry of Science and Technology MOST 108-2622-E-150-008-CC3 and National Formosa University 107AF06.

## References

- Beck C (1925) Apparatus to photograph the whole sky. *J Sci Instrum* 2:135–139. <https://doi.org/10.1088/0950-7671/2/4/305>
- Berge B, Peseux J (2000) Variable focal lens controlled by an external voltage: an application of electrowetting. *Eur Phys J E* 3:159–163. <https://doi.org/10.1007/s101890070029>
- Blum M, Büeler M, Grätzel C, Aschwanden M (2011) Compact optical design solutions using focus tunable lenses. *Proc SPIE* 8167:81670W. <https://doi.org/10.1117/12.897608>
- Brauer-Burchardt VK (2001) A new algorithm to correct fisheye-and strong wideangle-lens-distortion from single images. *Proc IEEE Int Conf Image Process* 1:225–228. <https://doi.org/10.1109/ICIP.2001.958994>
- Dong L, Agarwal AK, Beebe DJ, Jiang H (2006) Adaptive liquid microlenses activated by stimuli-responsive hydrogels. *Nature* 442:551–554. <https://doi.org/10.1038/nature05024>
- Edmund Optics Inc (2014) Imaging resources guide. <http://www.edmundoptics.com.tw/resources/application-notes/imaging/resolution/>
- Fang YC, Tsai CM (2008) Miniature lens design and optimization with liquid lens element via genetic algorithm. *J Opt A Pure Appl Opt* 10:075304. <https://doi.org/10.1088/1464-4258/10/7/075304>
- Fang YC, Tsai CM, Chung CL (2011) A study of optical design and optimization of zoom optics with liquid lenses through modified genetic algorithm. *Opt Express* 19:16291–16302. <https://doi.org/10.1364/OE.19.016291>
- Feng W, Zhang B, Roning J, Cao Z, Zong X (2011) An embedded omnidirectional vision navigator for automatic guided vehicles. *Proc. SPIE* 7878:1–12. <https://doi.org/10.1117/12.872281>
- Hao Q, Cheng X, Du K (2013) Four-group stabilized zoom lens design of two focal-length-variable elements. *Opt Exp* 21:7758–7767. <https://doi.org/10.1364/OE.21.007758>
- Hill R (1926) A lens for whole sky photography. *Proc Opt Conv* 2:878–883
- Huang Z, Bai J, Hou X (2010) A multi-spectrum fish-eye lens for rice canopy detecting. *Proc SPIE*. <https://doi.org/10.1117/12.869928>
- James JK, Martin LB (2000) Fish-eye lens designs and their relative performance. *Proc SPIE* 4093:360–369. <https://doi.org/10.1117/12.405226>
- Johnson RB, Feng C (1992) Mechanically compensated zoom lenses with a single moving element. *Appl Opt* 31:2274–2278. <https://doi.org/10.1364/AO.31.002274>
- Kienholz DF (2011) The design of a zoom lens with a large computer. *Appl Opt* 9:1443–1452. <https://doi.org/10.1364/AO.9.001443>
- Kuiper S, Hendriks BH, Huijbregts LJ, Hirschberg AM, Renders CA, Mav A (2004) Variable-focus liquid lens for portable applications. *Proc SPIE* 5523:100–109. <https://doi.org/10.1117/12.555980>
- Kuiper S, Hendriks BHW, Suijver JF, Deladi S, Helwegen I (2007) Zoom camera based on liquid lenses. *Proc SPIE*. <https://doi.org/10.1117/12.706779>
- Lin YS (2008) Design and analysis of ultra-wide angle lens system for car lens. National Taipei University of Science and Technology Institute of Optoelectronic Engineering, Taipei
- Lippmann G (1875) Relations entre les phénomènes électriques et capillaires. Gauthier-Villars, Paris
- Martinez T, Wick DV, Payne DM, Baker JT, Restaino SR (2004) Non-mechanical zoom system. *Proc SPIE* 5234:375–378. <https://doi.org/10.1117/12.510373>
- Mikš A, Novák J, Novák P (2008) Method of zoom lens design. *Appl Opt* 47:6088–6098. <https://doi.org/10.1364/AO.47.006088>
- Ning (2011) Compact fisheye objective lens. U.S. Patent No. 20090080093
- OmniVISION (2012) OV2722 CMOS Specifications. <https://data.sheetspdf.com/pdf-file/1088241/OmniVision/OV2722/1>
- Ren H, Wu ST (2007) Variable-focus liquid lens. *Opt Express* 15:5931–5936. <https://doi.org/10.1364/OE.15.005931>
- Ren H, Wu ST (2008) Tunable-focus liquid microlens array using dielectrophoretic effect. *Opt Express* 16:2646–2652. <https://doi.org/10.1364/OE.16.002646>
- Schulz H (1932) Fish eye lens. D.R. Patent No. 620538
- Sun JH, Hsueh BR, Fang YC, MacDonald J, Hu CC (2009) Optical design and multiobjective optimization of miniature zoom optics with liquid lens element. *Appl Opt* 48:1741–1757. <https://doi.org/10.1364/AO.48.001741>
- Varioptic Web (2006) <http://www.varioptic.com/en/index.php>
- Wick DV, Martinez T, Payne DM, Sweatt WC, Restaino SR (2005) Active optical zoom system. *Proc SPIE* 5798:151–157. <https://doi.org/10.1117/12.603475>
- Yen CY, Shih JM (2015) A study of optical design on 9× zoom ratio by using a compensating liquid lens. *Appl Sci* 5:608–621. <https://doi.org/10.3390/app5030608>
- Zhang W, Li D, Guo X (2013) Optical design and optimization of a micro zoom system with liquid lenses. *J Opt Soc Korea* 17:447–453. <https://doi.org/10.3807/JOSK.2013.17.5.447>
- Zheng JY, Li SG (2006) Employing a fish-eye for scene tunnel Scanning. *Asian Conf Comput Vis* 2006:509–518. [https://doi.org/10.1007/11612032\\_52](https://doi.org/10.1007/11612032_52)

**Publisher's Note** Springer Nature remains neutral with regard to jurisdictional claims in published maps and institutional affiliations.